Effect of external stress on nucleation of ellipsoidal precipitates in a Ti 20 wt% Mo alloy

Effect of external stress on nucleation of ellipsoidal ω precipitates in a Ti-20wt%Mo alloy

Ryoichi Monzen・Ryutaro Kawai・Chihiro Watanabe

R. Monzen[a]*

[a] Division of Mechanical Science and Engineering, Graduate School of Natural Science and Technology, Kanazawa University, Kakuma-machi, Kanazawa 920-1192, Japan

TEL: +81-76-234-4678

* Corresponding author, E-mail: monzen@se.kanazawa-u.ac.jp

R. Kawai[a]

[a] Division of Mechanical Science and Engineering, Graduate School of Natural Science and Technology, Kanazawa University, Kakuma-machi, Kanazawa 920-1192, Japan

TEL: +81-76-234-4681

C. Watanabe[a]

[a] Division of Mechanical Science and Engineering, Graduate School of Natural Science and Technology, Kanazawa University, Kakuma-machi, Kanazawa 920-1192, Japan

TEL: +81-76-234-4679

Abstract   The effects of an external stress on the formation of ellipsoidal ω phase precipitates have been examined for a Ti-20wt%Mo alloy aged at 300°C. Application of a tensile stress accelerates the nucleation of ω precipitates but a compressive stress does not significantly affect it. Estimates of the average misfit strains along the loading and the transverse directions, based on the misfit strains of ω precipitates, from measurements of the length change and the lattice parameter reveal preferential formation of specific ω variants among crystallographically-equivalent four ones, which depends on the sense of the applied stress. This is supported by the result of the dependence of the number density of an ω variant on its misfit strain along the loading direction. This result, together with the dependence of the formation of ω precipitates on the sense of the applied stress, can be well understood through the interaction energy due to the presence of misfit strains between the applied stress and ω precipitate.

Key words: Ti-Mo alloy; ω precipitates; nucleation; applied stress; misfit; interaction energy

Introduction

The effects of a directional stress during aging on the orientation distribution of precipitate structures have been examined widely for Al-Cu systems alloys [1-4]. For example, Eto et al [2] observed that application of the external stress during aging below 180°C induced the oriented precipitation of disk-shaped Guinier-Preston (GP) zones and plate-shaped θ' phase in single crystals of an Al-3.71Cu alloy (All compositions in this text are expressed by weight per cent, wt%). Tensile stress along the [001] axis produced the preferential formation of (100) and (010) variants of GP zones and θ', and compressive stress (001) variants. Using a two-step aging (aging at 80°C under stress and aging at 170°C under no stress) procedure, they showed that the stress-orienting effect was initiated and determined during the nucleation stage, namely the formation of GP[I], which will grow to θ' via GP[II].

On the other hands, Monzen et al [5] have shown by transmission electron microscopy (TEM) that application of an external stress during aging at 200°C induces the oriented precipitation of disk-shaped GP zones in single crystals of a Cu-0.9Be alloy. The disk-shaped GP zones consist of monolayers of Be atoms on the $\{100\}_\alpha$ planes. A compressive stress along the $[001]_\alpha$ direction assists preferential formation of the GP zones perpendicular to the stress axis and tensile stress induces the same parallel to the stress axis. They have also revealed that the effect of applied stress is on the nucleation process of GP zones. In addition, the misfit strains, $\varepsilon_{11}=\varepsilon_{22}$ and ε_{33}, of the GP zone in directions, respectively, parallel and perpendicular to the plate plane have been estimated from measurements of the length change and lattice parameter during aging. Moreover, Monzen et al [6] have examined the effects of an external stress on the nucleation and growth of disk-shaped γ'' phase for a Cu-1.2Be-0.1Co alloy aged at 320°C. The metastable γ'' phase is composed of alternate Be and Cu matrix layers parallel to the $\{100\}_\alpha$ planes. A compressive stress applied in the [001] direction during

3

aging preferentially accelerates the nucleation and growth of the γ" variant normal to the [001] axis among crystallographically-equivalent three ones. However, a tensile stress does not significantly affect the nucleation and growth of γ" precipitates. The acceleration of the nucleation and growth of the specific γ" variants can be well understood through the interaction energy between the stress acting on the γ" variants and their misfit strains. Prior to this work, Watanabe et al [7] already estimated the misfit strains, $\varepsilon_{11}=\varepsilon_{22}$ and ε_{33}, of the disk-shaped γ" precipitates from measurements of the length change and lattice parameter during aging.

In order to evaluate the effect of an applied tensile stress on the nucleation of ω precipitated phase in Ti-20Mo alloy specimens aged at 350°C, Nishizawa et al [8] have measured the number of ω precipitates in constant areas in the stress-free and stress-aged specimens, and concluded that a tensile stress applied during aging promotes the nucleation of ω precipitates. The structure of the ω phase in an aged Ti-14Mo alloy is hexagonal with a=0.2820 nm and c=0.4606 nm [9]. Since the ω precipitates have an ellipsoidal shape slightly elongated along <111>$_β$ of the β-Ti matrix [10], in contrast to the disk-shaped GP zones and γ" phase in Cu-Be alloys [5, 6] and the disk-shaped GP[1] zones and θ' phase in Al-Cu alloys [1-4], it is interesting to examine how crystallographically-equivalent four ω variants are formed under an applied external stress. We have found the stress-oriented nucleation of the ω precipitates, which depends on the sense of the applied stress, and furthermore found the promotion of the nucleation of ω precipitates under an applied tensile stress but almost no effect of an applied compressive stress on the nucleation, as will be shown later.

Experimental

Sheets of a Ti-20Mo alloy were provided by Daido Steel Co., Ltd. The alloy sheets were

cold-rolled to a 50% reduction in thickness and then spark-cut into specimen strips. For tensile aging, the specimens had a cross-section of 1 mm × 5 mm and a gage length of 20 mm. For compressive aging, the specimens had a cross-section of 2 mm × 5 mm and a gage length of 7 mm. All the specimens were solution-treated at 950 °C for 2 h in a vacuum and quenched into water. The solution treatment also caused complete recrystallization of the specimens. The solution-treated specimens were then aged at 300 °C for various times either under an applied stress of 450 MPa (stress aging) or under no stress (free aging). The applied stress of 450 MPa is about three fourths of the yield strength of the solution-treated specimen at 300 °C.

Length changes ε_T on aging were examined by measuring, with a micrometer, the distance between two scribed marks, about 4, 5 or 8 mm apart for the specimens stress-aged at 300 °C for 3 h and then free-aged at 350 °C for various times, or free-aged at 300 °C for 3 h and then free-aged at 350 °C for various times. The length change is defined as $\varepsilon_T = (l–l_0)/l_0$, where l_0 and l are the length between the two marks before and after aging, respectively. The measurement accuracy of length change is in the order of 10^{-5} in strain. An X-ray analysis was performed to measure the lattice parameters of the solution-treated and aged specimens. The diffractometer with a Cu target was used for the X-ray analysis.

Thin foils, 0.2 mm thick, for TEM observations were prepared by grinding the aged specimens with SiC papers and by electropolishing using a solution of 60 vol% methanol, 35 vol% 2-Butoxyethanol and 5 vol% perchloric acid at −20 °C and 15 V in a twin-jet electropolisher. Microscopy was performed using a JEOL 2010FEF microscope operated at 200 kV.

Results

Formation of ω precipitates under external stress

Figure 1a depicts a dark-field TEM image of the Ti-20Mo specimen aged at 300 °C for 12 h under a tensile stress of 450 MPa. Figure 1b shows the corresponding $[113]_\beta$ selected-area diffraction pattern (SADP). As shown schematically in Fig. 1c, reflections due to two ω variants, I and II, are present out of the four possible crystallographically-equivalent ω variants. The dark-field image was acquired using a reflection due to the variant I. The variants I and II aligned with the β-Ti matrix according to the following orientation relationship: $[1\bar{1}1]_\beta$ // $[0001]_{\omega1}$; $(\bar{2}\bar{1}1)_\beta$ // $(10\bar{1}0)_{\omega1}$; $(011)_\beta$ // $(\bar{1}2\bar{1}0)_{\omega1}$ and $[\bar{1}11]_\beta$ // $[0001]_{\omega2}$; $(\bar{1}\bar{2}1)_\beta$ // $(01\bar{1}0)_{\omega2}$; $(101)_\beta$ //$(\bar{2}110)_{\omega2}$. The variant I and II had an ellipsoidal shape elongated along $[4\bar{7}1]_\beta$ and $[\bar{7}41]_\beta$ on $(113)_\beta$.

Figure 2a, b, c shows dark-field images of the Ti-20Mo specimens, free-aged (FA), tensile-stress-aged (TSA) and compressive-stress-aged (CSA) at 300 °C for 12 h. These images were obtained with an incident electron beam along the [011] direction. Figure 2d is the corresponding [011] SADP. Reflections due to two ω variants, I and III, are present. The three dark-field images were taken using three reflections due to the variant I. The variant III exhibited the following orientation relationship to the β-Ti matrix: $[\bar{1}\bar{1}1]_\beta$ // $[0001]_{\omega3}$; $(\bar{2}\bar{1}1)_\beta$ // $(1\bar{1}00)_{\omega3}$; $(011)_\beta$ // $(11\bar{2}0)_{\omega3}$. All the four variants had an ellipsoidal shape elongated along $<111>_\beta$ with an aspect ratio of about 2, irrespective of application of external stress. Here, the shape of ω precipitates is assumed to be a spheroid described in the *x-y-z* coordinates by $x^2/r^2+y^2/r^2+z^2/l^2 \leq 1$, where $l \fallingdotseq 2r$. It may be noted in Fig. 2a, b, c that the precipitate sizes r and l for the TSA specimen are larger than those for the FA specimen, and also the sizes for the CSA specimen are slightly larger than those for the FA specimen.

Figure 3a, b, c display the number density N of the ellipsoidal ω precipitates, the lattice parameter of the β-Ti matrix measured as by X-ray analysis, and the average

precipitate sizes $\bar{r}$ and $\bar{l}$, each as a function of aging time t for the specimens TSA, CSA and FA at 300 °C. The number density of ω precipitates is defined as the volume fraction of precipitates divided by the average volume of a single precipitate. The volume fraction was determined by applying the lattice parameters of the TSA, CSA and FA specimens to the experimental data reported for the dependence of the lattice parameter on the Mo concentration ($\Delta a = -0.0002$ nm/at%) in the literature [11]. The concentration of Mo in the ω precipitates is assumed to be 10wt% equal to the equilibrium concentration of Mo at 300 °C in the Ti-Mo binary phase diagram [12]. Even if the Mo concentration in the precipitates is assumed to be 20wt% equal to the Mo concentration in the present alloy, the volume fraction estimated at each aging time is not significantly affected. The average volume of an ellipsoidal precipitate was obtained by measuring r and l of the four crystallographically-equivalent variants of ω precipitates. About 400 precipitates were used for measurements of l and r at each aging time.

Figure 3a demonstrates that the number density of ω precipitates is constant over a time span of 1.5 h (5.4×10^3 s) in the case of the TSA specimen, and over 3 h for the CSA and FA specimens. Thus the formation of the ω precipitates in the TSA, CSA and FA specimens is completed after either 1.5 or 3 h. More importantly, the number density of ω precipitates in the TSA specimen is higher than that in the FA specimen, indicating that the formation of ω precipitates is favored by applied tensile stress. There is, however, no significant difference in number density between the CSA and FA specimens. Moreover, it can be seen from Fig. 3c that aging under tension and compression accelerates the growth of the precipitates. The average sizes r and l of ω precipitates in the specimen FA at 300 °C follow a parabolic growth law (r and $l \propto t^{\frac{1}{2}}$), whereas aging at 300 °C under tension generates an increase in precipitate size that is linear with t. Consequently, while the growth of ω precipitates is governed by the diffusion of Mo atoms in ω precipitates from the interface between the β-Ti

7

matrix and the ω precipitates to the β-Ti matrix [12], precipitate growth is instead interface-controlled under tensile stress [6]. The result of a more detailed investigation of this phenomenon will be reported in a future paper.

Specimen length change

Figure 4 presents the length change ε_T along the loading direction (LD) and transverse direction (TD), plotted as a function of aging time t for the specimen at 300 °C for 3 h and then FA at 350 °C (TSA-FA), the specimen CSA at 300 °C for 3 h and then FA at 350 °C (CSA-FA), and the specimen FA at 300 °C for 3 h and then again FA at 350 °C (FA-FA). The specimens TSA, CSA and FA at 300 °C for 3 h each exhibits a slight decrease in length change. Length change along the LD and TD for the TSA-FA, CSA-FA and FA-FA specimens rapidly decreases and then eventually plateaus after about 53 h (1.908 x 10^5 s). The plateau value of ε_T along the LD for the TSA-FA specimen is larger than that along the TD for the same specimen, whereas, in the case of the CSA-FA specimen, the plateau value along the LD is smaller. In addition, the values of ε_T measured along several directions of the specimen FA at 300 °C for 3 h and then FA at 350 °C for 53 h were identical within experimental error, indicating that there was no anisotropy in length change of the FA-FA specimen. It should also be noted in Fig. 4 that length change along the LD for the specimens TSA and CSA at 300 °C for 3 h exhibits a slight decrease. This indicates that the creep strain due to dislocation motion does not contribute to the length change.

Figure 5 presents the dependence of the lattice parameter a of the β-Ti matrix on aging time t for the TSA-FA, CSA-FA and FA-FA specimens. The lattice parameter decreases with increasing aging time for the three specimens. Diffusion of Mo atoms in ω precipitates from the ω/β interface to the β-Ti matrix occurs as the ω precipitates grow [12]. Since the size of

8

Mo atoms is smaller than that of Ti atoms, the increase in Mo atoms within the β-Ti matrix causes the decrease in the lattice parameter. The lattice parameter of the TSA-FA specimen decreases more rapidly than that of the FA-FA specimen, although eventually the lattice parameters of both specimens converge on the same value of 0.3232 nm. This value is close to the lattice parameter, 0.3230 nm [11], of a β-Ti solid solution containing 38wt%Mo that is the equilibrium solubility of Mo in β-Ti at 350 °C in the Ti-Mo binary phase diagram [12]. The more rapid decrease in the lattice parameter of the TSA-FA specimen than the FA-FA specimen is attributed to the higher number density and the larger size of precipitates in the TSA-FA specimen (Fig. 3a, c). However, the lattice parameter of the CSA-FA specimen decreases slightly rapidly compared to that of the FA-FA specimen. This is attributable to the fact that the CSA-FA specimen has almost the same number density as the FA-FA specimen, and the slightly larger size of ω precipitates than the FA-FA specimen (Fig. 3a, c).

The specimen length-change ε_T along any direction can be written as functions of the average misfit strain ε_a along the same direction caused by the misfit strains of precipitates, the volume fraction f of the precipitates, and the dimensional change ε_l due to the increase in Mo atoms in the solid solution, as follows [7, 13]:

$$\varepsilon_T = f\varepsilon_a + (1-f)\varepsilon_1, \tag{1}$$

where $\varepsilon_1 = (a-a_0)/a_0$. Here a_0 and a are the lattice parameters of the specimens before and after aging.

We are able to estimate the average misfit strains ε_{aL} and ε_{aT} along the LD and TD for the TSA-FA and CSA-FA specimens, as well as the average misfit strain ε_{aF} for the FA-FA specimen. A value for f of 0.14 was obtained by applying the values $a_0 = 0.3253$ nm and $a = 0.3232$ nm before and after aging at 350 °C for 53 h (Fig. 5) to the experimental data regarding the dependence of the lattice parameter on Mo concentration [11]. The Mo

concentration in the ω precipitates was assumed to be 10wt%, as noted above. Table 1 summarizes the resulting values of ε_{aL}, ε_{aT} and ε_{aF} for the specimens TSA and then FA at 350 °C for 53 h (TSA-FA'), CSA and then FA at 350 °C for 53 h (CSA-FA'), and FA and then FA at 350 °C for 53 h (FA-FA'). These values were estimated from the value of ε_T in Fig. 5, as well as from f and ε_l. The value of $\varepsilon_{aF} = 0.010$ is in good agreement with the misfit strain of ε_c = 0.0096, calculated from the lattice parameters $a = 0.3232$ nm for the β-Ti matrix and $a =$ 0.2835 nm and $c = 0.4676$ nm for the ω precipitates, as determined by X-ray analysis after aging at 350 °C for 53 h, using the following equation:

$$\varepsilon_c = \frac{1}{3}\left(\frac{V_\omega}{V_\beta} - 1\right). \tag{2}$$

Here V_ω and V_β are the molar volumes of the ω precipitates and β matrix, respectively. The measured values of a and c for the ω precipitates are close to the values $a = 0.2820$ nm and c = 0.4606 nm for the ω precipitates in a Ti-14Mo alloy [9]. The ε_c value of 0.010 also is nearly identical to the value of $\varepsilon_c = 0.0088$ obtained by Hickman [14] from the lattice parameters of the ω precipitates and β matrix using Eq. 2. For the TSA-FA' specimen, $\varepsilon_{aT} = 0.008 < \varepsilon_{aF} =$ $0.010 < \varepsilon_{aL} = 0.028$, while for the CSA-FA' specimen, $\varepsilon_{aL} = 0.004 < \varepsilon_{aF} = 0.010 < \varepsilon_{aT} = 0.016$. These data indicate that tensile stress preferentially aids the formation of specific ω variants out of the crystallographically-equivalent four ones, having positive misfit strains along the LD greater than $\varepsilon_{aF} = 0.010$, and that compressive stress induces the preferential formation of specific ω variants with smaller positive and/or negative misfit strains along the LD. Below, the dependence of the number density of the ω variants on the misfit strain along the LD is examined for the specimens TSA, CSA and FA at 300 °C for 12, 48 and 48 h, respectively.

Misfit strain and number density of ω variants

We often observed grains in which the $(113)_\beta$ plane was nearly parallel to the surfaces of the TSA, CSA and FA specimens. The number densities of the ω variants I and II were determined by taking dark-field images using reflections due to these variants I and II in the $[113]_\beta$ SADPs (see Fig. 1), and measuring the thicknesses of TEM foils using thickness fringes. In addition, the misfit strains of the variants I and II along the LD on $(113)_\beta$ were obtained by measuring the angle ϕ between the LD and the elongated $[4\bar{7}1]_\beta$ or $[\bar{7}41]_\beta$ direction of the variant I or II on $(113)_\beta$ (see Fig. 1a), then calculating the LD, i.e. $[h\ k\ l]_\beta$ and $[p\ q\ r\ s]_\omega$, under the condition of $h^2 \leq 225$, $k^2 \leq 225$, $l^2 \leq 225$, $p^2 \leq 225$, $q^2 \leq 225$, $r^2 \leq 225$ and $s^2 \leq 225$, and furthermore estimating the spacings of the planes perpendicular to $[h\ k\ l]_\beta$ and $[p\ q\ r\ s]_\omega$.

Figure 6 presents the number density N of variants I and II, plotted as a function of the misfit strain ε_M of each variant along the LD for the TSA, CSA and FA specimens. The value of 9.5×10^{22} m^{-3} obtained for the FA specimen when multiplied by four equals 3.8×10^{23} m^{-3}, which is in agreement with the value of $N = 4.1 \times 10^{23}$ m^{-3} obtained for the FA specimen from Fig. 3a. Several large misfit strains, such as 0.24 and 0.29, are present in Fig. 6. However, the actual misfit strains may be small, since a large misfit strain can be relieved by an array of misfit dislocations at the interface between different phases [6, 7, 15, 16, 17]. The values of N for the TSA specimen are larger than those for the FA specimen when $\varepsilon_M > 0$, but are smaller when $\varepsilon_M < 0$. On the other hand, the values of N for the CSA specimen are larger than those for the FA specimen when $\varepsilon_M < 0$, but are smaller when $\varepsilon_M > 0$. It is also noted that the average of the N values obtained for the TSA specimen is larger than that for the CSA specimen. This fact agrees with the observation that the number density of ω precipitates in the TSA specimen is higher than that in the CSA specimen (Fig. 3a).

Discussion

The origin of the dependences of the formation of ω precipitates (Fig. 3a), the relationship between the number density of ω variants and the misfit strain along the LD (Fig. 6) and the average misfit strains along the LD and TD (Table 1) on the sense of the applied stress can be understood to arise through the interaction energy between an external stress σ_{ij} and a misfit strain ε_{ij} (stress-free transformation strain). That is, the cause of the present results is understood to be due to the work done by the external stress during the nucleation of ω precipitates. The interaction energy F_I is expressed as [18]:

$$F_I = -V\sigma_{ij}\varepsilon_{ij}, \tag{3}$$

where V is the volume of the ω precipitate. According to a classical nucleation theory [19], the interaction energy F_I affects the nucleation rate R as written by:

$$R \propto \exp\left(-\frac{\left(G^* + F_I^*\right)}{kT}\right), \tag{4}$$

where G^* is the activation energy for nucleation in absence of a stress, F_I^* is the interaction energy associated with nucleation of the ω precipitate of a critical nucleus volume, k is Boltzmann's constant and T is the absolute temperature.

Eqs. 3 and 4 predict that applied tensile stress promotes the nucleation of ω precipitates because the average misfit strain $\varepsilon_{aF} = 0.010$ for the FA specimen, but compressive stress does not affect it. This prediction is in agreement with the result shown in Fig. 3a. Similarly, it may be expected from Eqs. 3 and 4 that tensile and compressive stress promote the nucleation of a ω variant when the misfit strain of the variant along the LD is positive and negative respectively. This is coincident with the dependence of the number density of ω variants on the misfit strain in Fig. 6. Moreover, Eqs. 3 and 4 predict that, for the TSA specimen, the average misfit strain ε_{aL} along the LD is larger than $\varepsilon_{aF} = 0.010$ for the FA

specimen, and, for the CSA specimen, $\varepsilon_{aL} < 0.010$. This is the case, as shown in Table 1.

Conclusions

1. Application of tensile stress during aging at 300 °C promotes the nucleation of ellipsoidal ω precipitates in a Ti-20wt%Mo alloy, but compressive stress does not essentially affect the same.

2. From measurements of the length change and the lattice parameter during aging, the average misfit strains along the loading and the transverse directions, caused by the misfit strains of ω precipitates, have been estimated for the tensile-stress-aged and compressive-stress-aged specimens. The estimates reveal that specific ω variants among crystallographically equivalent ones are preferentially formed, depending on the sense of the applied stress. This is supported by the result of the dependence of the number density of ω variants formed under the applied stress on the misfit strain of the variants along the loading direction.

3. The dependences of the nucleation of ω precipitates and the formation of specific ω variants on the sense of the applied stress can be understood through the interaction energy due to the presence of misfit strains between the applied stress and ω precipitate.

References

1. Hosford WF, Agrawal SP (1975) Effect of stress during aging on the precipitation of θ' in Al-4 Wt pct Cu. Metall Mater Trans A 6A:487-491

2. Eto T, Sato A, Mori T (1978) Stress-oriented precipitation of G. P. Zones and θ' in an Al-Cu alloy. Acta Metal 26:499-508

3. Skrotzki B, Shiflet GJ, Starke Jr EA (1996) On the effect of stress on nucleation and growth of precipitates in an Al-Cu-Mg-Ag alloy. Metall Mater Trans A 27A:3431-3444

4. Zhu AW, Starke Jr EA (2001) Stress aging of Al–xCu alloys: experiments. Acta Metall 49:2285-2295

5. Monzen R, Watanabe C, Seo T, Sakai T (2005) Effect of applied stress on precipitation of Guinier–Preston zones in a Cu–0.9 wt.% Be single crystal. Phil Mag Lett. 85:603-612

6. Monzen R, Okawara S, Watanabe C (2012) Stress-assisted nucleation and growth of γ'' and γ' precipitates in a Cu–1.2 wt%Be–0.1 wt%Co alloy aged at 320°C. Phil Mag 92:1826-1843

7. Watanabe C, Sakai T, Monzen R (2008) Misfit strains of precipitated phases and dimensional changes in Cu–Be alloys. Phil Mag 88:1401-1410

8. Nishizawa H, Sukedai E, Liu W, Hashimoto H (1998) Effect of applied stress on formation of ω-Phase in β-Ti alloys. Mater Trans JIM 39:609-612

9. Silcock JM (1958) An X-ray examination of the ω phase in TiV, TiMo and TiCr. Acta Metall 6:481-493

10. Fontaine DD, Paton NE, Williams JC (1971) The omega phase transformation titanium alloys as an example of displacement controlled reactions. Acta Metall 19:1153-1162

11. Kun S, Xuezhong Y, Erdong W, Dongfeng C, Cheng G (2006) Neutron diffraction study of the deuterides of Ti-Mo alloys. Physica B 385-386:141-143

12. Fontaine DD (1988) Simple models for the omega phase transformation. Metall Trans A 19A:169-175

13. Monzen R, Terazawa T, Watanabe C (2010) Influence of external stress on discontinuous precipitation behavior in a Cu-Ag alloy. Metall Mater Trans A 41A:1936-1941

14. Hickman BS (1969) Omega phase precipitation in alloys of titanium with transition Metals. Trans Metall Soc AIME 245:1329-1336

15. Pond RC, Celotto S, Hirth JP (2003) A comparison of the phenomenological theory of martensitic transformation with a model based on interfacial defect. Acta Mater 51:5385-5398

16. Pond RC, Hirth JP (1994) Defects at surfaces and interfaces. Solid State Phys 47:287-365

17. Miyazawa T, Fujii T, Onaka S, Kato M (2011) Shape and elastic state of nano-sized Ag precipitates in a Cu-Ag single crystal. J Mater Sci 46:4228-4235

18. Eshelby JD (1957) The determination of the elastic field of an ellipsoidal inclusion, and related problems. Proc R Soc A 241:376-396

19. Volmer M, Weber A (1926) Keimildung in ubersattigetn gebilden. Z Phys Chem. 119:277-301

Figure and Table Captions

Fig. 1 (a) Dark-field TEM image of ω precipitates in a Ti-Mo specimen aged at 300 °C for 12 h under a tensile stress of 450 MPa. LD=Loading Direction. **(b)** [113]$_\beta$ SADP corresponding to **(a)**. **(c)** Schematic illustration of the previous [113]$_\beta$ SADP. ○= variant I reflections, △= variant II reflections

Fig. 2 (a), (b), (c) Dark-field TEM images of ω precipitates in Ti-Mo specimens aged at 300 °C for 12 h under no stress, a tensile stress and a compressive stress. The zone axis is along [011]$_\beta$. **(d)** Corresponding [011]$_\beta$ SADP

Fig. 3 Aging time t dependence of **(a)** the number density N of ω precipitates, **(b)** the lattice parameter a of β-Ti matrix and **(c)** the average sizes $\bar{r}$ and $\bar{l}$ of ω precipitates in Ti-Mo specimens, TSA (450MPa), CSA (450MPa) and FA at 300 °C. Representative error bars are shown

Fig. 4 Aging time t dependence of the length change ε_T for Ti-Mo specimens, TSA at 300 °C for 3 h and FA at 350 °C (TSA-FA), CSA at 300 °C for 3 h and FA at 350 °C (CSA-FA), and FA at 300 °C for 3 h and FA at 350 °C (FA-FA). Representative error bars are shown

Fig. 5 Aging time t dependence of the lattice parameter a of β-Ti matrix for Ti-Mo specimens, TSA-FA, CSA-FA and FA-FA. Representative error bars are shown

Fig. 6 Number density N of ω variants in Ti-Mo specimens, TSA, CSA and FA at 300 °C for 12, 48 and 48 h respectively as a function of the misfit strain ε_M of the variants along the LD.

Table 1 Average misfit strains ε_{aL} and ε_{aT} along the LD and TD obtained by length-change measurements for Ti-Mo specimens TSA at 300 °C for 3 h and FA at 350 °C for 53 h (TSA-FA') and CSA at 300 °C for 3 h and FA at 350 °C for 53 h (CSA-FA'), and average misfit strain ε_{aF} for a specimen FA at 300 °C for 3 h and FA at 350 °C for 53 h (FA-FA')
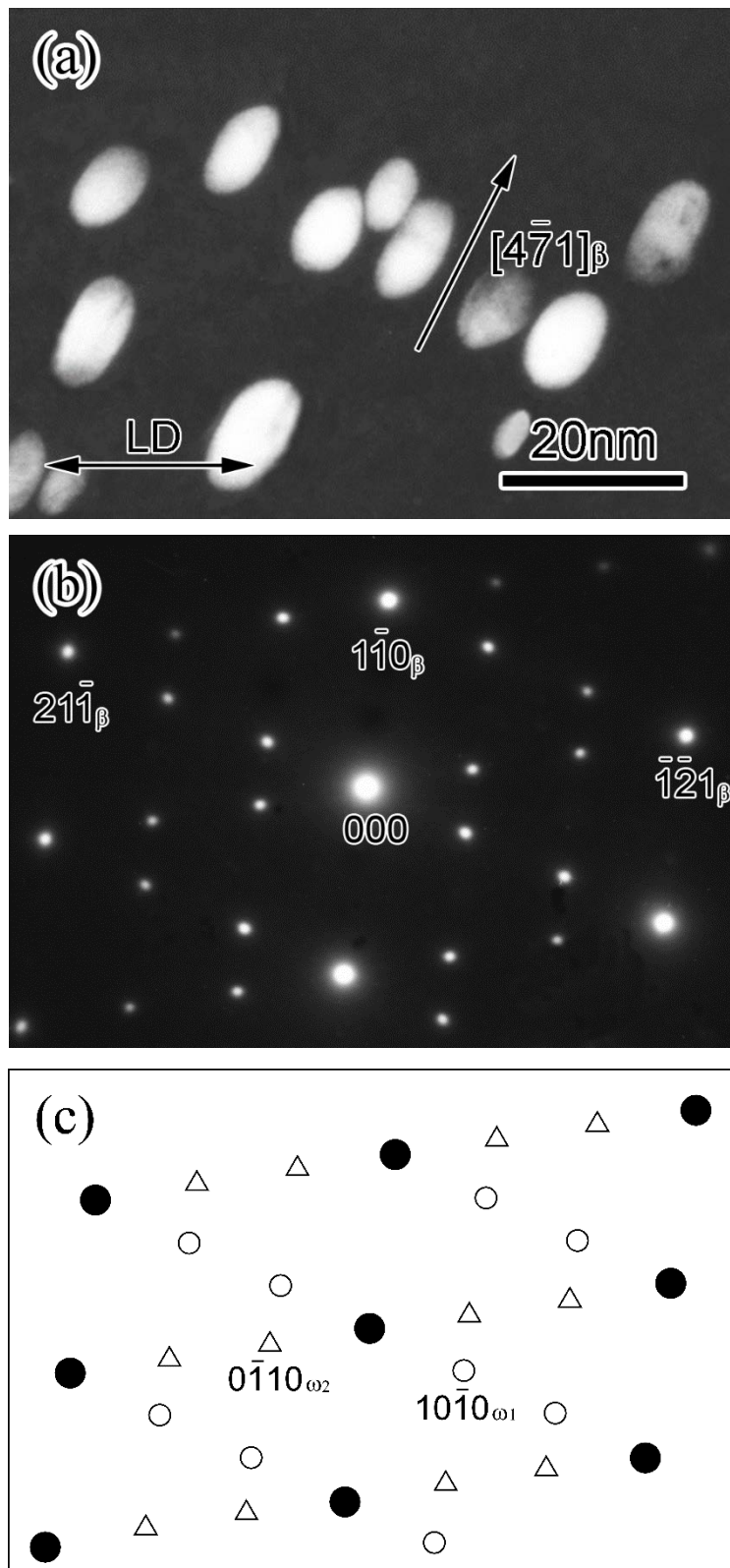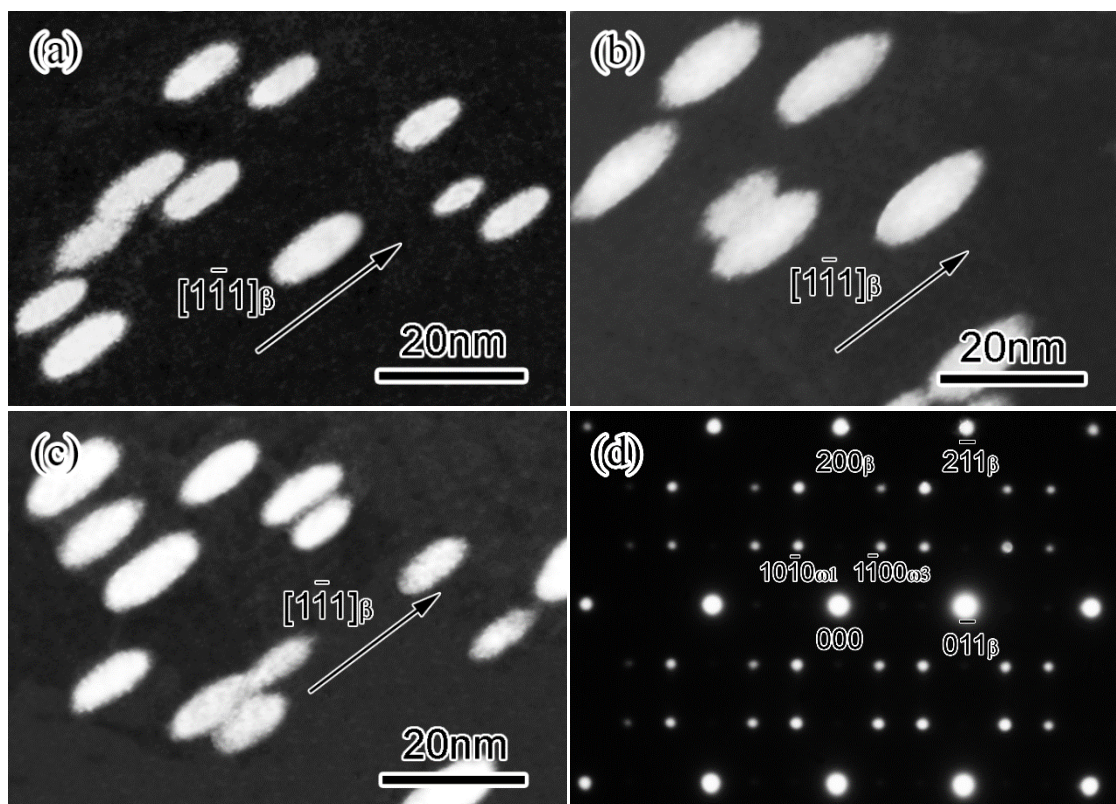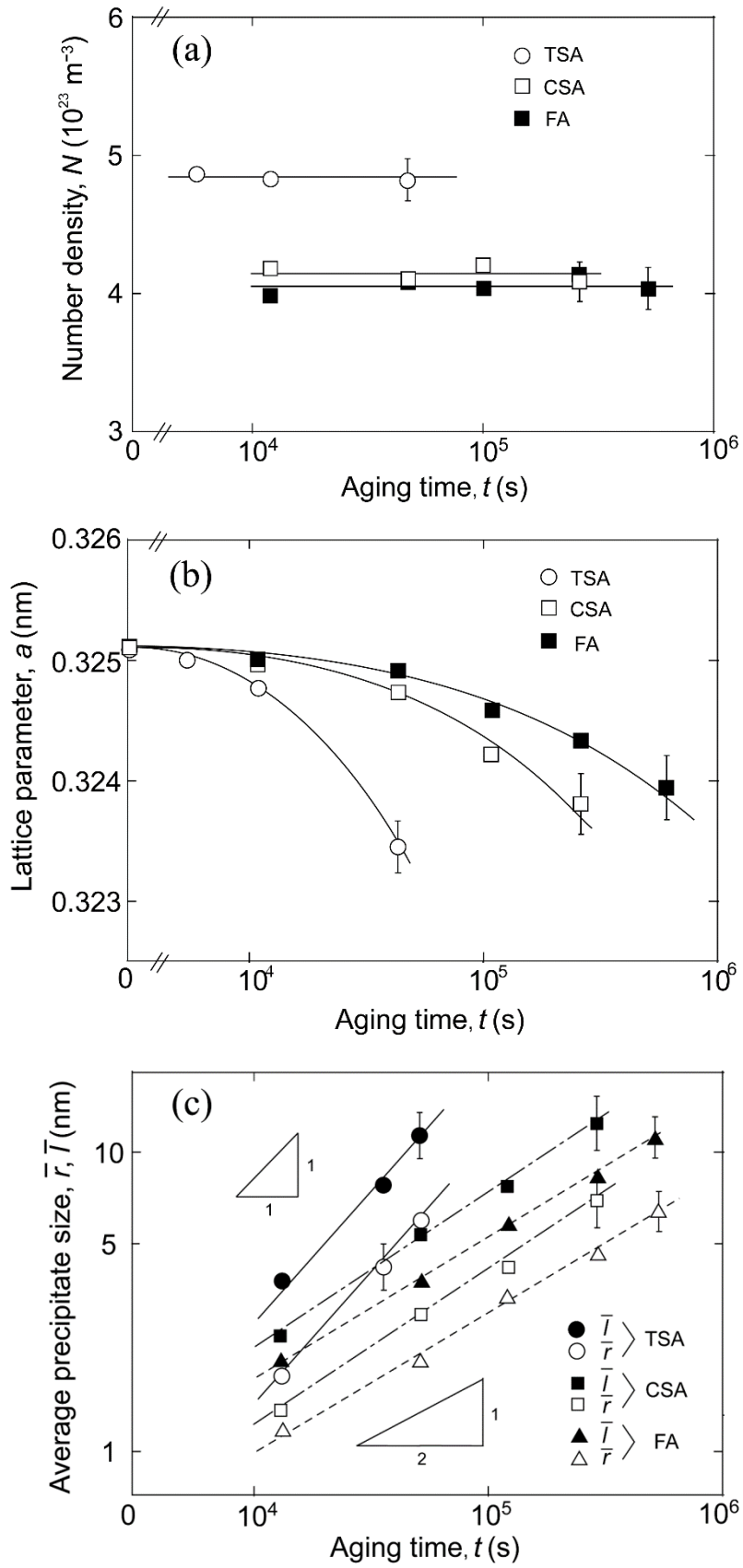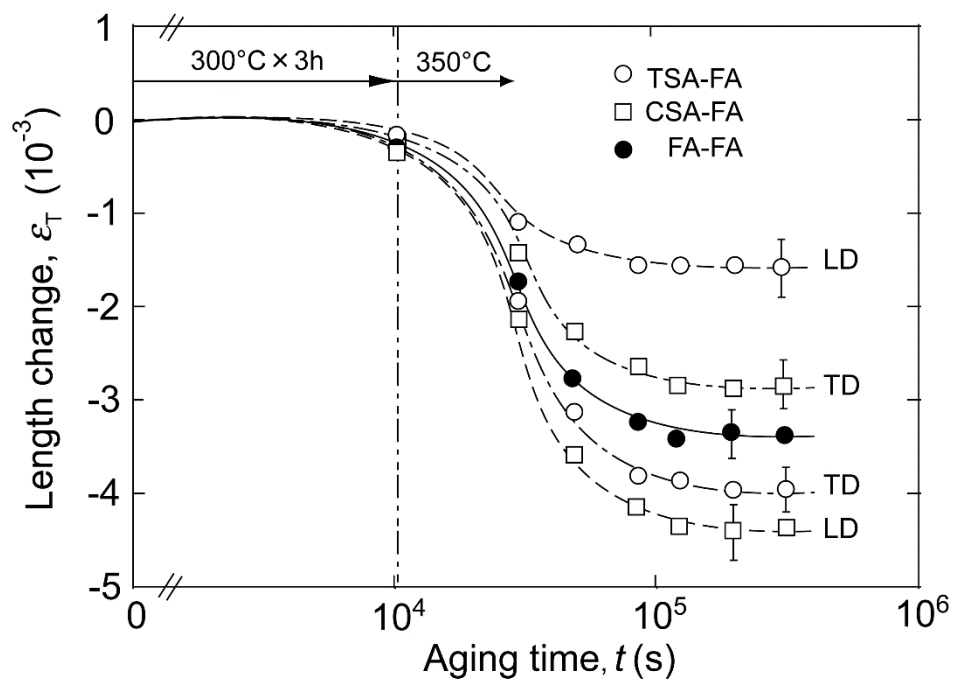
Fig. 1

Fig. 2

Fig. 3

Fig. 4
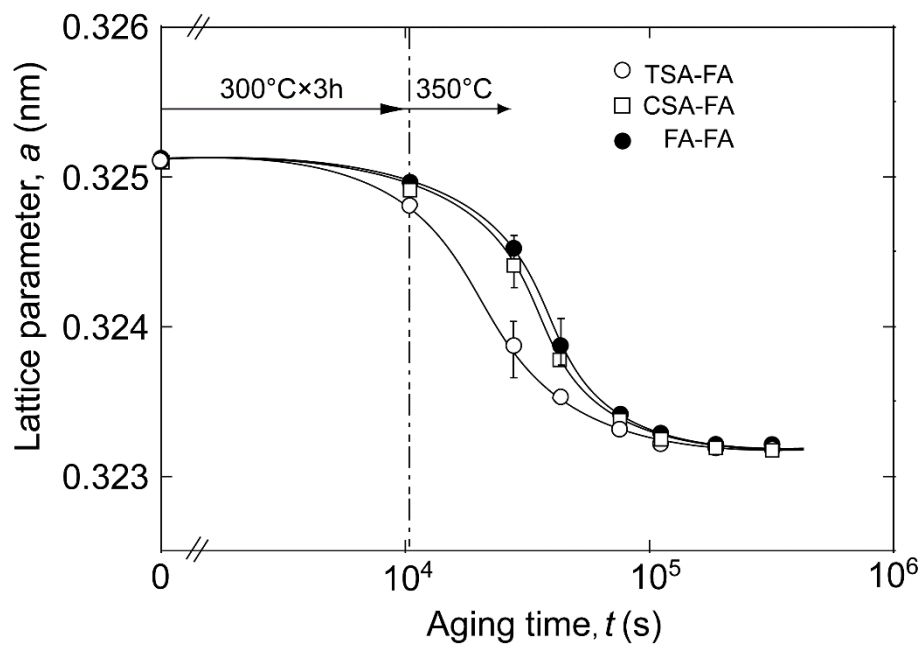
Fig. 5
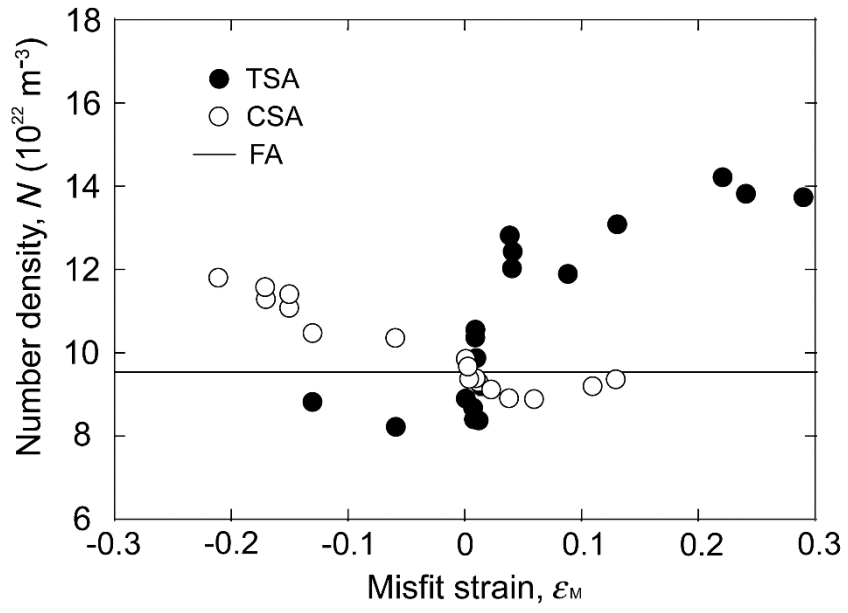
Fig. 6

Table 1

Specimen	ε_{aL}	ε_{aT}
TSA-FA'	0.028	0.008
CSA-FA'	0.004	0.016
FA-FA'	0.010	